ELSEVIER

International Journal of Mass Spectrometry 222 (2003) 329–349

International Journal of Mass Spectrometry

www.elsevier.com/locate/ijms

Collision-induced dissociation and theoretical studies of K^+ complexes with ammonia: a test of theory for potassium ions

Christopher Iceman, P.B. Armentrout*

Department of Chemistry, University of Utah, Salt Lake City, UT 84112-0850, USA

Received 3 May 2002; accepted 16 July 2002

In honor of Jack Beauchamp, a tremendous scientist, mentor, and friend.

Abstract

The sequential bond energies of K^+ with ammonia are determined using collision-induced dissociation (CID) with xenon gas in a guided ion beam tandem mass spectrometer. The kinetic energy dependences of the CID cross-sections are analyzed to give 0 and 298 K bond energies for the successive loss of ammonia after accounting for multiple collisions, internal energy, and dissociation lifetimes. We also consider whether to treat torsional motions as vibrations or rotations and whether to include the ion–dipole potential in the treatment of the transition state for dissociation. Bond energies at 0 K (in kJ/mol) of $K^+(NH_3)_x$ are determined for $x = 1$–5 as 79 ± 7, 69 ± 6, 59 ± 5, 46 ± 6, 31 ± 11, respectively, decreasing with increasing x as expected for electrostatic bonds. These dissociation energies agree quantitatively with literature values available from equilibrium studies for $x = 1$–4 (mean absolute deviation $= 2 \pm 1$ kJ/mol). This agreement suggests that these systems can be used to test theory for K^+ complexes, and therefore several levels of theory are explored here. The $x = 1$–5 complexes are calculated to adopt high symmetry structures where the ligands bind directly to the metal. We find that trends in the experimental bond energies are accurately reproduced at the MP2(full)/6-311+G(2d,2p)//MP2(full)/6-31G(d) and B3LYP/6-311+G(2d,2p)//B3LYP/6-31G levels, although the values are generally low, by an average of 4 ± 3 kJ/mol ($8 \pm 3\%$). Values obtained using the effective core potentials of Hay–Wadt and Stuttgart–Dresden on potassium are less satisfactory and underestimate experiment by an average of 9 ± 6 kJ/mol ($14 \pm 7\%$). (Int J Mass Spectrom 222 (2003) 329–349)

Keywords: Ammonia; Collision-induced dissociation; K^+; Guided ion beam mass spectrometry; Bond dissociation energies

1. Introduction

The biological importance of potassium is well known. In ion channels of the nervous system, the binding of potassium to ligands is an essential part of the mechanism for message transport [1]. Because of the steric requirements of these small ion channels, potassium transport may be inhibited or enhanced by its complexation to various sized ligands, in particular, water [2–4]. Therefore, an understanding of the solvation of potassium ions may provide useful information regarding the functionality of this metal ion in biological systems, in addition to being of fundamental interest.

In the present work, we examine the solvation of K^+ by ammonia, a system for which there are several experimental studies in the literature [5–8]. High-pressure mass spectrometry (HPMS) was used by

* Corresponding author. E-mail: armentrout@chem.utah.edu

1387-3806/02/$ – see front matter
PII S1387-3806(02)00954-5

Davidson and Kebarle to determine the temperature dependent equilibrium constant for formation of $K^+(NH_3)$ [5]. Castleman extended such HPMS studies to one to four ammonia ligands, determining the sequential bond enthalpies [6]. Early collision-induced dissociation (CID) studies using a triple quadrupole instrument were done by Marinelli and Squires to obtain the bond energy for the single ligand complex [7]. Matrix IR spectroscopic studies of the potassium ammonia complex have also been investigated [8]. These spectroscopic studies probed the trends in the intensities of the ν_{1-4} bands of alkali metal ammonia complexes primarily to investigate the effects of charge transfer.

Recently, our laboratory has used threshold collision-induced dissociation (TCID) methods to measure bond dissociation energies (BDEs) of a variety of ligands to the alkali metal cations [9–11]. In the present work, we extend these studies to obtain quantitative BDEs for the $K^+(NH_3)_x$ systems for up to $x = 5$ ligands. We find good agreement with values for $x = 1$–4 obtained from the HPMS studies of Castleman, indicating that these complexes may be used as benchmarks for other experimental work and for theory. On the experimental side, we use this comparison to decide whether torsional motions in the $K^+(NH_3)_x$ complexes are best treated as vibrations or rotations. In addition, we examine whether the ion–dipole potential should be included in our description of the transition state for dissociation, as used in our statistical analysis of the kinetics of the CID process.

Several theoretical calculations have also been done on potassium ion ammonia complexes [12–14]. $K^+(NH_3)$ was studied by Berthod and Pullman [12] and by Magnusson and Moriarty [14], whereas Kaupp and Schleyer examined the complexes containing one and two ammonia molecules [13]. The focal point of these computational studies was to assess both the geometric and energetic properties of the systems. In the present work, we examine the structures and energetics of the five $K^+(NH_3)_x$, $x = 1$–5, complexes at several levels of theory. We are particularly interested in whether calculations employing effective core potentials on potassium can accurately reproduce the bond energies for these species as some difficulties were observed in our work on $K^+(C_6H_6)_x$, $x = 1$ and 2 [9]. A comparison between experiment and theory allows an evaluation of several theoretical methods and suggests the need for improvements.

2. Experimental and computational details

2.1. Experimental procedures

The experimental cross-sections for the CID of the $K^+(NH_3)_x$ complexes are measured using a guided ion beam tandem mass spectrometer. A complete description of the instrument is given in the literature [15–17]. Potassium cation–ammonia clusters are generated in a 1-m long flow tube with 0.5–0.7 Torr of helium mixed with ~10% argon at a flow rate of 6500–7500 sccm. Potassium ions are created by a continuous dc-discharge source, which comprises a water-cooled metal rod made from tantalum with a cavity containing potassium metal. The cathode is held to a voltage of about −2 kV. $K^+(NH_3)_x$ complexes are formed by associative three-body reactions of the potassium ions with ammonia introduced to the flow about 50 cm downstream of the dc discharge. The ion complexes experience 0.5×10^5–1×10^5 collisions with the surrounding room temperature buffer gas, which should thermalize the ions both rotationally and vibrationally. The complexes should be in their ground electronic states with internal energies described well by a Maxwell–Boltzmann distribution at this temperature. This has been shown to be a good assumption in other works [18–22].

The ions are extracted from this source and focused into a magnetic momentum analyzer for mass selection. These mass selected ionic complexes are then decelerated to a specific kinetic energy and focused into an octopole ion guide that contains the ions in the radial direction using radio-frequency electric fields [23]. The octopole passes through a static gas cell containing xenon at pressures between 0.05 and 0.2 mTorr, which limits the possibility of multiple collisions. The octopole guide efficiently collects scattered reactant

and product ions and allows them to drift to the end of the octopole. There they are extracted, focused into a quadrupole mass filter, and then detected by a secondary electron-scintillator-phototube detector and standard pulse counting techniques. Ion intensities are converted to absolute cross-sections that have uncertainties of about ±20% resulting from uncertainties in the collision gas pressure and reaction path length [15].

Collision energies are converted from the laboratory (lab) frame into the center-of-mass (CM) frame by the equation $E_{CM} = E_{lab}m/(m + M)$ where m is the mass of the reactant neutral and M is the mass of the reactant ion. All energies reported below are in the CM frame unless otherwise noted. The absolute zero and distribution of the ion kinetic energies are determined using the octopole ion guide as a retarding potential analyzer as previously described [15]. Because the reaction zone and energy analysis region are physically the same, ambiguities in the energy analysis resulting from contact potentials, space charge effects, and focusing aberrations are minimized [15]. The distribution of ion kinetic energies is nearly Gaussian with a fwhm typically between 0.2 and 0.3 eV (lab) for these experiments. The uncertainty in the absolute energy scale is ±0.05 eV (lab).

2.2. Data analysis

The kinetic energy dependence of the CID cross-sections is modeled using Eq. (1):

$$\sigma(E) = \sigma_0 \sum \frac{g_i(E + E_i - E_0)^n}{E} \quad (1)$$

where σ_0 is a scaling factor that is independent of the energy, E is the relative translational energy of the reactants, E_0 is the threshold for reaction at zero Kelvin, and n is an adjustable fitting parameter that describes the efficiency of collisional energy transfer [17]. This summation is over the rotational and vibrational states of the reactant complexes having excitation energies, E_i, and populations, g_i, where $\sum g_i = 1$. We use the Beyer–Swinehart algorithm [24–27] to calculate the ro-vibrational energy distribution of the ionic complexes at 298 K using molecular constants scaled from ab initio calculations, as detailed below. Uncertainties in the molecular constants from the calculations are estimated by scaling the frequencies by ±10%. This method is consistent with studies done by Pople and co-workers [28] and DeFrees and McLean [29] to cover the range of scale factors necessary to draw calculated frequencies into agreement with experimental frequencies.

We also consider the possibility that the collisionally activated complexes do not dissociate on the time scale of the experiment, about 5×10^{-4} s [17]. This is achieved by including Rice–Ramsperger–Kassel–Marcus (RRKM) statistical theory [27] for unimolecular dissociation into Eq. (1), as detailed elsewhere [20,30]and given in Eq. (2).

$$\sigma(E) = \left(\frac{n\sigma_0}{E}\right) \sum_i g_i \int_{E_0 - E_i}^{E} [1 - e^{-k(\varepsilon + E_i)\tau}] \times (E - \varepsilon)^{n-1}\, d\varepsilon \quad (2)$$

Here, ε is the energy deposited into the complex by the collision with Xe, τ is the average experimental time available for dissociation (the ion time-of-flight from the collision cell to the quadrupole mass analyzer), and $k(\varepsilon + E_i) = k(E^*)$ is the RRKM unimolecular dissociation rate constant. In the limit that $k(E^*)$ is faster than the time-of-flight of the ions, this integration recovers Eq. (1). Recent work has shown that the distribution of deposited energies used in Eq. (2) is consistent with experiment [17] and properly characterized by the parameter n. The RRKM analysis requires ro-vibrational frequency sets for the energized molecules and transition states. Because these complexes have largely electrostatic interactions, the transition states are assumed to be loose and to occur at the centrifugal barrier for interaction of $K^+(NH_3)_{x-1} + NH_3$, a phase space limit (PSL). Thus, the transition state has molecular parameters equivalent to the products, as discussed elsewhere [30].

The external 2D rotors of the energized complex are assumed to be adiabatic and centrifugal effects are included as outlined by Waage and Rabinovitch [31]. As originally formulated by Rodgers et al. [30], the

average unimolecular dissociation rate constant for a statistical distribution of rotational quantum numbers was determined using Eq. (3):

$$\langle k(E^*, J)\rangle = \frac{\sum_{J=0}^{J_{max}} k(E^*, J) g_J \rho_{vr}(E^* - E_R(J))}{\sum_{J=0}^{J_{max}} g_J \rho_{vr}(E^* - E_R(J))} \quad (3)$$

where J is the rotational quantum number, $g_J = (2J + 1)$ is the degeneracy of the 2D rotor, $E_R(J)$ is the energy in the 2D external rotation of the complex, $\rho_{vr}(E^* - E_R(J))$ is the density of ro-vibrational states of the complex at the available energy not tied up in the 2D external rotation, and J_{max} is the maximum value possible for the rotational quantum number determined by energy conservation. This average dissociation rate constant is then used to calculate the dissociation probability, $[1 - e^{-\langle k(E^*,J)\rangle\tau}]$. We will refer to this model as the average rate constant model. DeTuri and Ervin [32] later pointed out that the most precise treatment of single channel CID processes was probably to average the entire dissociation probability over the statistical distribution of rotational quantum numbers, Eq. (4), and use this expression in Eq. (2).

$$\langle 1 - e^{-k(E^*,J)\tau}\rangle = \frac{\sum_{J=0}^{J_{max}} [1 - e^{-k(E^*,J)\tau}] g_J \rho_{vr}(E^* - E_R(J))}{\sum_{J=0}^{J_{max}} g_J \rho_{vr}(E^* - E_R(J))} \quad (4)$$

We refer to this model as the average dissociation probability model here.

In our previous work, the centrifugal barrier to dissociation has been assigned on the basis of a long-range potential given by the ion-induced dipole interaction. In cases like the present systems, the long-range interaction should include the potential associated with the interaction of the ion and the permanent dipole moment of the ligand. Here we alter our treatment of the centrifugal barrier to include a long-range ion-locked dipole attraction, chosen for simplicity. This limit, combined with ignoring the ion–dipole potential, should provide adequate representations of the effects of a dipole on the long-range potential and the dissociation behavior. Because the ligand starts aligned in the complex, the ion-locked dipole potential may be a reasonable limit to consider and is given by $V_{LD} = -e\mu_D/4\pi\varepsilon_0 r^2$, where μ_D is the dipole moment of the neutral product, e is the charge of an electron, ε_0 is the permittivity of a vacuum, and r is the distance between the products. Thus, the effective potential is given by

$$V_{eff}(r) = \frac{L^2}{2\mu r^2} - \frac{\alpha e^2}{8\pi\varepsilon_0 r^4} - \frac{e\mu_D}{4\pi\varepsilon_0 r^2} \quad (5)$$

where L is the orbital angular momentum of the products, μ is the reduced mass of the products, and α is the polarizability of the neutral product. To find the height of the centrifugal barrier, $V_{eff}(r^*)$, which is equated with the rotational energy of the transition state, $E_R^\dagger(J)$, we set the derivative of $V_{eff}(r)$ with respect to r equal to zero, solve for the position of the barrier, r^*, and substitute back into the expression for $V_{eff}(r)$. This gives Eq. (6):

$$E_R^\dagger(J) = V_{eff}(r^*) = \frac{\pi\varepsilon_0}{2\alpha e^2}\left[\frac{L^2}{\mu} - \frac{e\mu_D}{2\pi\varepsilon_0}\right]^2 \quad (6)$$

We then equate L with the rotational angular momentum of the energized molecule, $[J(J+1)\hbar^2]^{1/2}$, which is related to the rotational energy of the energized molecule, $E_R(J) = hcBJ(J+1)$, where B is the rotational constant of the energized molecule. Thus, $L^2 = \hbar^2 E_R(J)/hcB$, such that the height of the centrifugal barrier is determined by various molecular parameters and the rotational energy of the energized molecule, for which several assumptions are possible, as outlined previously [30]. It can be shown that the addition of the dipole term to the potential moves the centrifugal barrier to larger r and decreases its height, leading to a smaller kinetic shift. (In assessing expression (6), it is important to realize that the term in square brackets can be negative when the ion–dipole term, $e\mu_D/2\pi\varepsilon_0$, is more attractive than the orbital angular momentum term, $L^2/\mu = \hbar^2 E_R(J)/hcB\mu$. Under these conditions, the height of the centrifugal barrier, $V_{eff}(r^*)$, is zero, rather than being given by expression (6).)

The model presented in Eq. (1) applies to reactions that are driven by translational motion [33], and reproduces reaction cross-sections accurately in many atom–diatom and polyatomic reactions [34,35], as

well as in CID experiments [11,18,20,22,30,36–40]. In addition, we have recently demonstrated that the cross-section form given in Eq. (1) is consistent with direct measurements of the energy transferred in collisions between $Cr(CO)_6^+$ and Xe [17], a result that provides increased confidence in the use of this model to obtain accurate thermodynamic information from CID thresholds. Before comparison to the data, this model is convoluted over the kinetic energy distributions of the reactants [15]. The parameters, E_0, σ_0, and n, are then optimized by a non-linear least-squares analysis. Included in the error of the E_0 measurement are variations in the thresholds associated with different data sets (minimum of 3), those from scaling vibrational frequencies up and down by 10%, and the uncertainty in the absolute energy scale. When RRKM analysis is included in the modeling, an uncertainty associated with scaling the flight time available for dissociation (5×10^{-4} s) up and down by a factor of 2 is also included.

After convolution over the kinetic energy distributions of the reactants, the threshold model of Eq. (1) includes all sources of energy available to the reactants. The assumption that all energies are capable of contributing to dissociation is reasonable because the rotational and vibrational energy of the reactants is repartitioned throughout the ion complex upon collision with Xe. By definition, the threshold is the minimum amount of energy needed to dissociate the reactants to products with an internal temperature of 0 K. These various assumptions have been investigated previously [11,18,20,22,30,36] and found to provide satisfactory thermochemical results. Therefore, threshold energies obtained from analysis of the data using Eq. (1) are converted into bond energies under the assumption that E_0 is the energy difference between the reactants and products at 0 K [22]. This assumes that there are no activation barriers for the reaction that exceed the endothermicity of dissociation. For the metal–ligand dissociations studied here [34], this is reasonable because of the attractive long-range ion–dipole and ion-induced dipole interactions and because these processes are simple heterolytic bond fissions [41].

2.3. Computational details

Gaussian 98W [42] was used to carry out calculations on the ligand and metal–ion–ligand complexes for $K^+(NH_3)_x$ where $x = 1$–5. Geometry optimizations and vibrational analyses were initially conducted at the MP2(full)/6-31G(d) level [43–45]. Hoyau et al. [46] and we [10,47] have shown that this level of theory provides an adequate description of sodium cation complexes and magnesium cation complexes. Initial geometry optimizations led to geometries having imaginary frequencies corresponding to rotations of the ammonia ligands around the K–N axis. Constraining the geometries to symmetric equilibrium structures eliminates these imaginary frequencies, verifying that the symmetric geometries correspond to true minima on the potential energy surfaces. When vibrational frequencies are used to model our data or to estimate thermal corrections, they are scaled by a factor of 0.9646, as discussed elsewhere [48]. The vibrational frequencies and rotational constants of the optimized geometries can be found in Tables 1 and 2.

To accurately determine the absolute energy of the complexes, single point energy calculations at the MP2 (full)/6-311+G(2d,2p) level were performed using the optimized MP2(full)/6-31G(d) geometries. Corrections for zero-point energy (ZPE) and basis set superposition error (BSSE) were included to give a 0 K bond energy, D_0. This procedure utilizes the full counterpoise approximation [49,50] and has previously been shown to provide a reasonable description of other alkali metal–ligand systems [9,10,46]. For the smaller ($x \leq 3$) clusters, the BSSE approached 3 kJ/mol and the maximum BSSE was 4 kJ/mol for $K^+(NH_3)_5$. However, we also consider the possibility that the full counterpoise approximation overestimates the BSSE by reporting values without corrections for BSSE.

To augment these computational studies, we also calculated geometries and single point energies using the same sequence of MP2 calculations but utilizing effective core potentials (ECPs) on the potassium ion. Both the relativistic ECPs of Hay–Wadt (HW) [51], equivalent to the Los Alamos ECP (LANL2DZ) basis set, and Stuttgart–Dresden (SD) [52] were used

Table 1
Vibrational frequencies (cm^{-1}) of $K^+(NH_3)_x$ complexes and internal energies (eV) at 300 K[a]

Species	E_{int}	Torsional modes	K^+-ligand frequencies	Ligand frequencies
NH_3	0.001			1118, 1693(2), 3383, 3534(2)
$K^+(NH_3)$	0.031		215, 420(2)	1299, 1690(2), 3359, 3484(2)
$K^+(NH_3)_2$	0.117	11	14(2), 171, 226, 391(2), 401(2)	1280(2), 1690(4), 3362(2), 3490(4)
$K^+(NH_3)_3$	0.180	14(2), 20	16, 19(2), 164, 200(2), 338, 362(2), 384(2), 391	1263(3), 1690(6), 3364(3), 3495(6)
$K^+(NH_3)_4$	0.271	4, 21(3)	25(2), 30(3), 156, 181(3), 306(3), 352(2), 371(3)	1237(3), 1244, 1690(8), 3367(4), 3501(8)
$K^+(NH_3)_5$	0.373	17(2), 19, 49, 50	9(2), 44(2), 47(3), 125, 144, 166(3), 229(2), 272, 274(2), 336, 352(4)	1207, 1210, 1214(2), 1221, 1689(10), 3370(5), 3507(10)
$K^+(NH_3)_4(NH_3)$	0.380	9, 17(2)	13, 20, 24(2), 29, 80, 90, 135, 162, 176, 183(2), 198, 205, 268, 290, 309, 321, 342, 349, 355, 405, 463, 529	1224, 1229, 1232, 1235, 1253, 1689(8), 1714, 1723, 3342, 3348, 3366, 3368(2), 3474, 3480, 3498, 3502(3), 3503, 3504, 3506(2)

[a] Degeneracies in parentheses. Frequencies calculated at MP2(full)/6-31G(d) level.

Table 2
Rotational constants (cm^{-1}) of $K^+(NH_3)_x$ complexes[a]

Species	Symmetry	1D	2D	Internal rotors
NH_3	C_{3v}	6.32	9.87	–
$K^+(NH_3)$	C_{3v}	6.39	0.17	–
$K^+(NH_3)_2$	D_{3d}	3.19	0.058	12.63
$K^+(NH_3)_3$	C_{3h}	0.038	0.074	12.63, 6.46, 3.19
$K^+(NH_3)_4$	T_d	0.041	0.041	12.63(2), 3.19(2)
$K^+(NH_3)_5$	C_{3h}	0.036	0.031	12.63(2), 6.46(2), 3.19
$K^+(NH_3)_4(NH_3)$	C_s	0.051	0.021	12.63, 6.35, 3.19

[a] Degeneracies in parentheses. Calculated at MP2(full)/6-31G(d) level.

for this purpose. Further, we substituted the B3LYP density functional for MP2 theory in the geometry optimizations using the 6-31G(d) basis set and single point energies using the 6-311+G(2d,2p) basis set. This utilizes Becke's three parameter functional [53] and the correlation functionals of Lee, Yang, and Parr (LYP) [54]. Finally, we also calculated MP2(full)/6-311+G(2d,2p) single point energies using the B3LYP/6-31G(d) geometries. In all of these cases, separate BSSE calculations in the full counterpoise limit were performed, but zero point energy corrections used the same set of scaled MP2 frequencies calculated as noted above.

3. Results

The interactions of potassium ion–ammonia complexes with Xe were studied from thermal to fairly high energies (3–7 eV in the center-of-mass frame) in order to observe all possible dissociation products and to check for any unusual dissociations or anomalies in the CID data. In addition, scans were performed over a wide range of masses to ensure that no contaminants were present in either reactant. Xenon was used as the collision partner because of its efficiency of translational energy transfer [55,56]. The Xe pressure dependence of the CID cross-sections was investigated over the range of 0.05–0.2 mTorr and found to be small for all of the CID systems studied (within the stated 20% experimental uncertainty). Nevertheless, extrapolations to zero Xe pressure were done to provide rigorous single collision cross-sections for analysis in all cases. For the case of $K^+(NH_3)_5$, the primary product intensity at the highest pressure examined (0.2 mTorr) was greater than that of the reactant ion beam, indicating that tertiary collisions are probable. To avoid difficulties associated with this, we collected

data between 0.02–0.1 mTorr to allow for a true linear extrapolation of the data sets to zero pressure. Unfortunately, the intensity of this ion was also the smallest of those examined here (~5000 counts/s) such that the data for this complex are particularly noisy.

The cross-section data for the CID of $K^+(NH_3)_x$, $x = 1$ and 4, with Xe are shown in Fig. 1, and are representative of the behavior of all complexes. In all cases, the dominant reactions observed are the CID process (7).

$$K^+(NH_3)_x + Xe \rightarrow K^+(NH_3)_{x-1} + NH_3 + Xe \quad (7)$$

For $x > 1$, we also observe sequential loss of additional ligands at higher energies, Fig. 1b. The cross-sections for reaction (7) in all five systems increase steeply from a threshold energy that gradually decreases with increasing cluster size. Because of the lower thresholds and the larger physical size

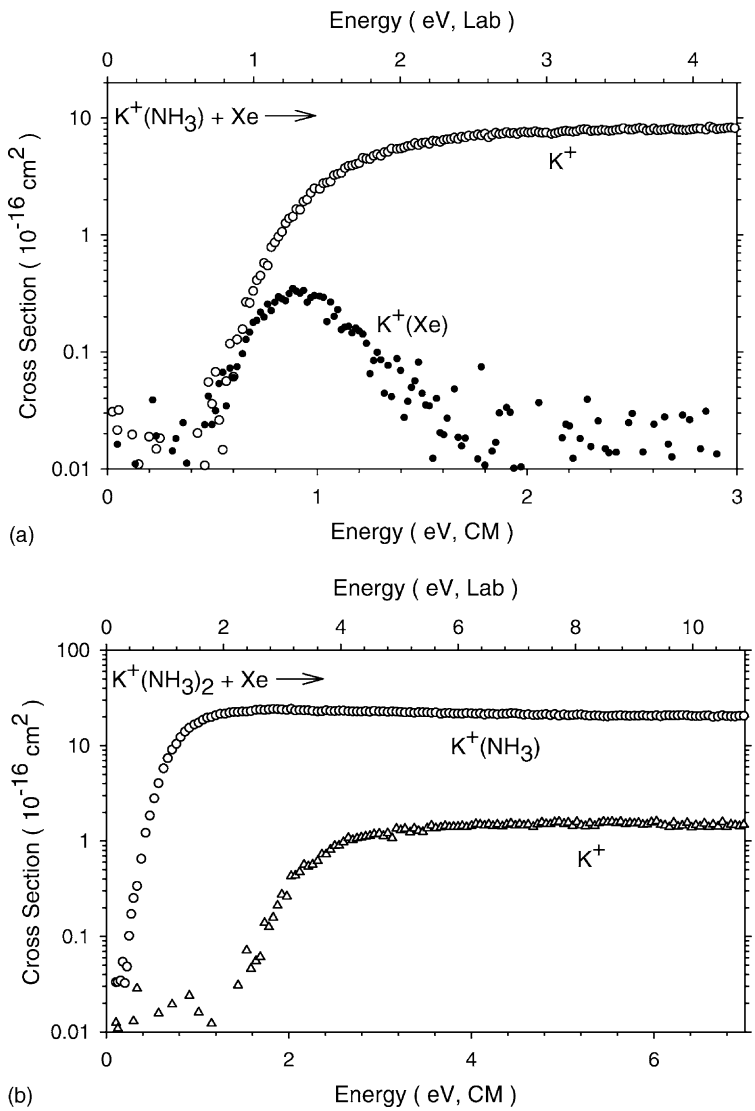

Fig. 1. Cross-sections for collision-induced dissociation of $K^+(NH_3)_x$ where $x = 1$–5 (parts (a–e), respectively) with Xe as a function of kinetic energy in the center-of-mass frame (lower x-axis) and the laboratory frame (upper x-axis).

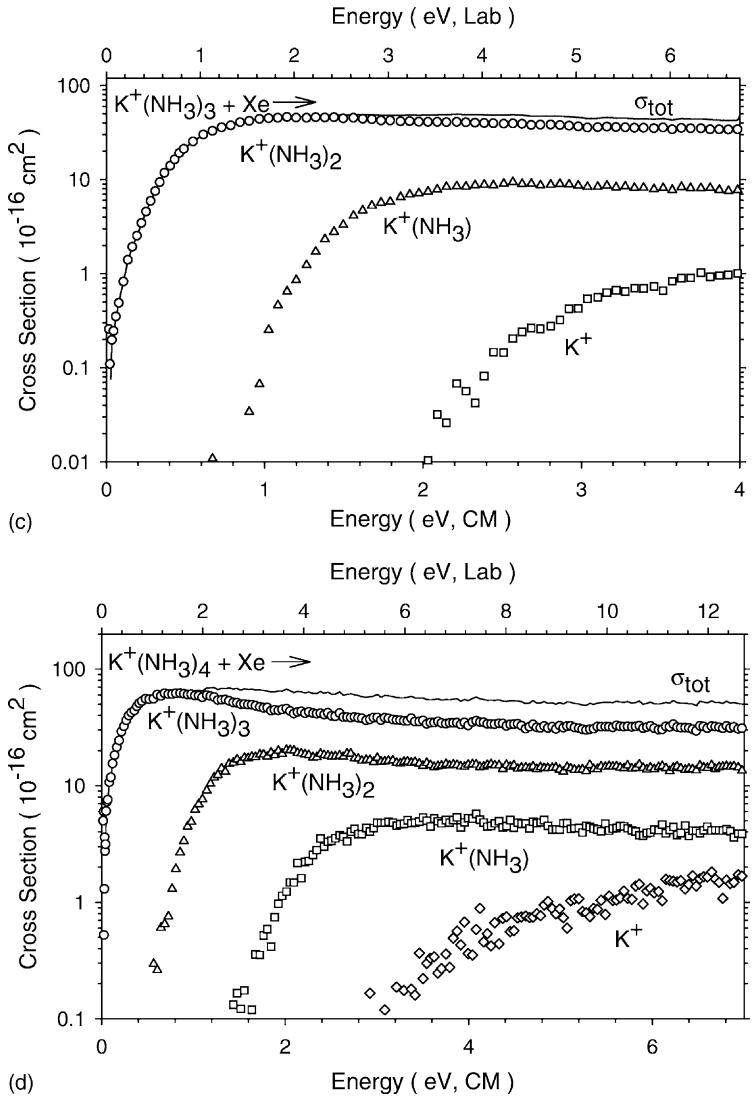

Fig. 1. (*Continued*).

of the complexes, the magnitudes of the reaction cross-sections increase with *x*. The cross-sections level off at higher energies and then decline as additional ligands can be lost. The energetic behavior observed for the secondary ligand loss channels indicates that these reactions occur by sequential loss of the ammonia ligands in all cases.

The only other process observed was ligand exchange to produce KXe^+ in the $K^+(NH_3)$ reaction (Fig. 1a). This cross-section does not exceed 5×10^{-17} cm^2, and hence it is not surprising that analogous processes were not observed for any of the larger complexes.

3.1. Threshold analysis

The RRKM analysis of the CID cross-sections is treated using a loose phase space limit (PSL) model for

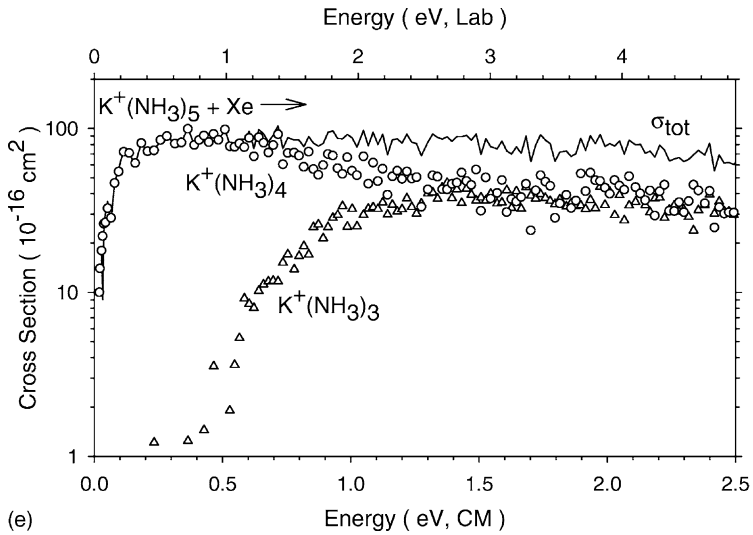

Fig. 1. (*Continued*).

the transition state, as described above. Many previous studies have shown that this model allows an accurate description of the magnitude of the kinetic shifts in the CID of metal–ligand complexes [11,30,36,38–40]. The total reaction cross-section for ligand dissociation was modeled for all complexes (although this is equivalent to only the primary dissociation process for $x = 1$ and 2) because the shapes of the cross-sections for the $K^+(NH_3)_{x-1}$ channels are influenced by the subsequent decompositions in the $x = 4$ and 5 complexes.

The CID cross-sections were analyzed using two different sets of frequencies for the molecular parameters used in the RRKM calculations. In one set, all frequencies are taken directly from theory, Table 1, which is expected to be accurate for all higher frequencies. However, several of the very low frequency motions ($<50\,cm^{-1}$) were found to correspond to internal torsions of the ligands rotating about their K–N bonds. Thus, the second set of molecular parameters treats these motions as free rotors and replaces the calculated vibrational frequencies with rotational constants for such motions, as listed in Table 2. These values are determined using moment of inertia calculations described in detail elsewhere [27].

For each of the two different frequency sets, we also analyzed the data with and without accounting for kinetic shifts using RRKM rates. Optimized thresholds obtained for all four types of analysis are listed in Table 3. Kinetic shifts for the two sets of frequencies were similar for the $K^+(NH_3)_x$, $x = 1$–4 complexes, and varied from 0.0 eV for $x = 1$ to 0.09 eV for $x = 4$. These comparisons are provided in Figs. 2 and 3. For the largest cluster, $x = 5$, differences in the two frequency sets are more noticeable with kinetic shifts of 0.29 eV when all vibrational frequencies are used and 0.25 eV when rotors are used for the torsional motions. (Smaller kinetic shifts, Table 3, are obtained if the cluster is analyzed using parameters appropriate for the alternate 4,1 structure, see below.) Our initial bias in the appropriate treatment is to incorporate the lifetime effects and treat the torsions as rotors; however, the present study allows an independent assessment of which of these treatments provides the best results by comparison with the HPMS experimental results of Castleman for the $x = 1$–4 complexes [6]. Comparison of our results with HPMS values adjusted to 0 K (as detailed below) can be summarized by the mean absolute deviations (MAD). To consider the lifetime effects, we examine the $x = 3$ and 4 clusters because lifetime effects are essentially absent for $x = 1$ and 2. Without lifetime effects included, the MAD is 12 ± 1 kJ/mol when all vibrational frequencies are

Table 3
Optimized parameters of Eq. (1) for CID of $K^+(NH_3)_x$ ($x = 1$–5) complexes with Xe[a]

Reactant ion	Product ion	# torsion	σ_0[b]	n[b]	Average rate constant				Average dissociation probability	$\Delta S^{\ddagger}_{1000}$ (PSL) (J/(mol K))
					E_0 (no RRKM) (eV)		E_0 (PSL) (eV)		E_0 (PSL) (eV)	
					Torsions	Rotors	Torsions	Rotors	Rotors	
$K^+(NH_3)$	K^+	0	13 (1)	1.0 (0.1)	0.83 (0.07)	0.83 (0.07)	0.83 (0.07)	0.83 (0.07)	0.82 (0.07)	17 (2)
$K^+(NH_3)_2$	$K^+(NH_3)$	1	44 (1)	0.9 (0.1)	0.75 (0.06)	0.73 (0.07)	0.74 (0.06)	0.73 (0.06)	0.71 (0.06)	4 (3)
$K^+(NH_3)_3$	$K^+(NH_3)_2$	3	66 (1)	0.8 (0.1)	0.69 (0.05)	0.65 (0.06)	0.66 (0.05)	0.63 (0.05)	0.62 (0.05)	24 (2)
$K^+(NH_3)_4$	$K^+(NH_3)_3$	4	84 (1)	0.9 (0.1)	0.64 (0.07)	0.58 (0.06)	0.55 (0.06)	0.54 (0.06)	0.48 (0.06)	36 (3)
$K^+(NH_3)_5$	$K^+(NH_3)_4$	5	95 (1)	0.8 (0.1)	0.66 (0.13)	0.62 (0.10)	0.37 (0.13)	0.37 (0.12)	0.32 (0.12)	−10 (4)
$K^+(NH_3)_4(NH_3)$	$K^+(NH_3)_4$	3	94 (2)	0.8 (0.1)	0.61 (0.14)	0.56 (0.12)	0.41 (0.12)	0.42 (0.11)	0.33 (0.11)	30 (7)

[a] Uncertainties in parentheses. Threshold uncertainties reported as 2σ.
[b] Fitting parameters (σ_0 and n) are reported for data modeled with average dissociation probability values.

used and 8 ± 1 kJ/mol when rotors are used for the torsions. When lifetime effects are included, the results improve to a MAD of 6 ± 2 kJ/mol when all vibrations are used and 5 ± 1 kJ/mol when rotors are used for the torsions. Similar trends are observed when all clusters $x = 1$–4 are considered with the best MAD being 3 ± 2 kJ/mol for modeling with lifetime effects and torsions treated as rotors. This comparison makes it clear that lifetime effects are critical to modeling especially in the larger clusters, whereas the use of rotors rather than vibrations for the torsional modes has a more modest effect. Theoretical values could also be used

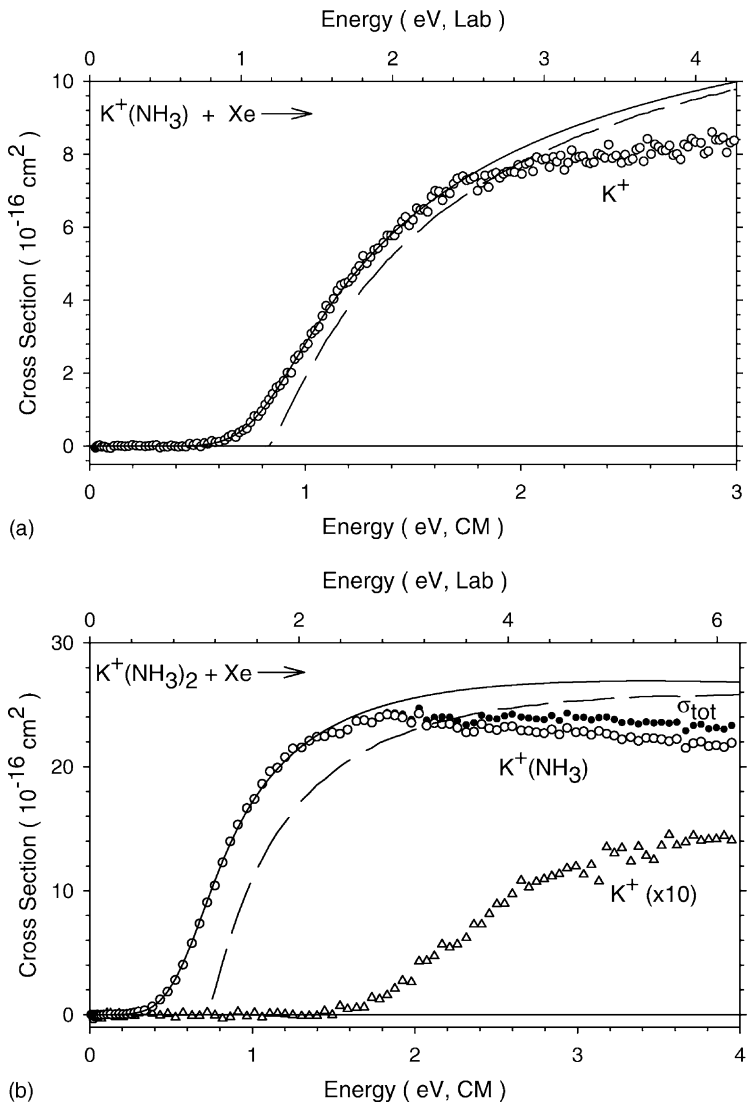

Fig. 2. Zero pressure extrapolated cross-sections for collision-induced dissociation of $K^+(NH_3)_x$ where $x = 1$–5 (parts (a–e), respectively) with Xe in the threshold region as a function of kinetic energy in the center-of-mass frame (lower *x*-axis) and the laboratory frame (upper *x*-axis). Solid lines show the best fit to the data using the model of Eq. (1) convoluted over the neutral and ion kinetic and internal energy distributions. Dashed lines show the model cross-sections in the absence of experimental kinetic energy broadening for reactions with an internal energy of 0 K.

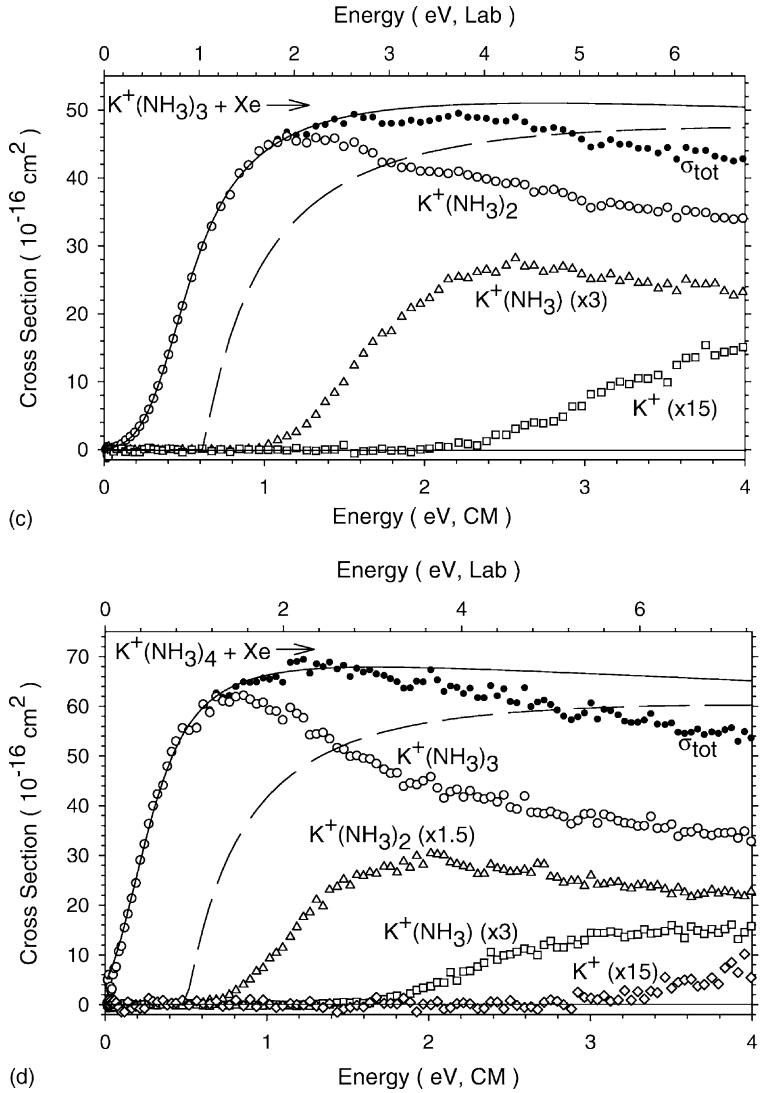

Fig. 2. (*Continued*).

to provide an independent measure of which analysis treatment is most accurate, but the results are the same.

We also examined the effects of our treatment of the 2D external rotational energy of the complex by explicitly considering both the average rate constant model and the average dissociation probability model, as described in detail above. Threshold values for these two models including lifetime effects and using rotors for the torsional modes are compared in Table 3. The other models (e.g., using vibrations as the torsions and no lifetime treatments) show relative threshold energies that match those shown for the average rate constant model. It can be seen that the use of the average dissociation probability model provides slightly lower thresholds with the difference increasing for larger complexes, a consequence of larger kinetic shifts. This is because the dissociation probability

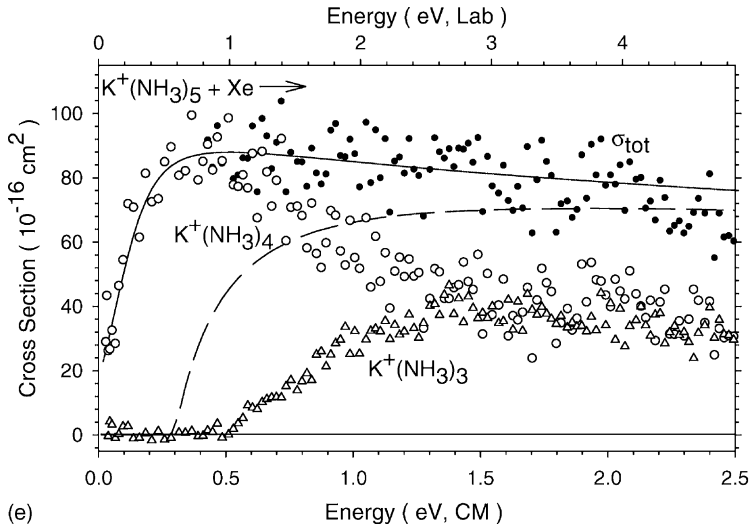

Fig. 2. (*Continued*).

drops rapidly with increasing rotational energy of the complex (because the centrifugal barrier is higher) such that the average dissociation probability is lower than the dissociation probability calculated for the average total rate constant. The differences between the two models are well within the experimental errors cited and should be system dependent. Nevertheless, the comparison of the values obtained with the average dissociation probability model and the HPMS results shows a slightly improved MAD of 2 ± 1 kJ/mol. Fig. 2 shows that the model of Eq. (1) using an average dissociation probability including lifetime effects and torsional rotors reproduces the data for all five systems over extended ranges of energy and magnitude. Similar reproduction of the data can be obtained with the average rate constant model.

As noted above, we modeled the data assuming a PSL TS located at the centrifugal barrier. The results reported in Table 3 were obtained using a barrier calculated using just the ion-induced dipole potential, as in all previous reaction systems we have studied. If the ion-locked dipole potential is included in the determination of the centrifugal barrier, this should provide a limit to the influence that the dipole will have on the dissociation behavior. Differences in the analysis results for the models with and without dipoles included (for both the average rate constant and average dissociation probability models) were very small, <2 kJ/mol, well within our experimental error. The locked dipole gives a higher threshold indicating that there is less kinetic shift, consistent with smaller centrifugal barriers located at longer internuclear distances. The average dissociation probability model gives slightly larger differences (by only about 1 kJ/mol) between thresholds with and without the dipole included. Although the inclusion of the ion–dipole potential is not influential in the present case, it should be interesting in future work to monitor this in cases where the dipole is considerably larger than for ammonia (1.47 D) [57].

Finally, a reviewer wondered if our consideration of these various factors should also include the anharmonicities of the vibrational frequencies, in particular for those "frustrated translational" modes that lead to dissociation. We estimated the anharmonicities using the Morse potential expression, $\omega_e x_e = \omega_e^2/4D_e$, where ω_e is the appropriate vibrational frequency (of which there are x for each $K^+(NH_3)_x$ complex) and D_e is the bond dissociation energy from the bottom of the potential well. Including these anharmonicities did not change the threshold energies for the $x = 1$–4 complexes, whereas the $x = 5$ complex exhibited a shift of

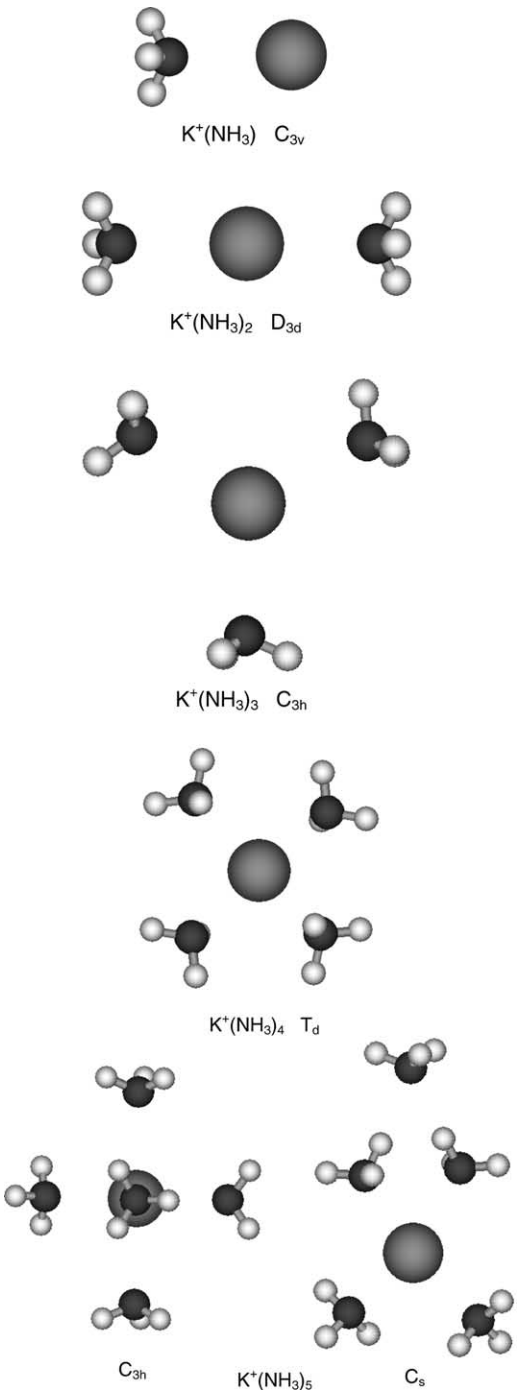

Fig. 3. Ground-state geometries of $K^+(NH_3)_x$ where $x = 1$–5. All structures were optimized at the MP2(full)/6-31G(d) level of theory.

about 0.01 eV. Thus, effects of these anharmonicities are essentially negligible in the present case.

A useful measure of the looseness of the transition state is represented by the entropies of activation, $\Delta S^{\ddagger}$, listed in Table 3 along with other modeling parameters. These values are calculated at 1000 K using the molecular parameters given in Tables 1 and 2, a rigid-rotor/harmonic oscillator approximation, and standard formulae. These are generally found to be positive, correctly reflecting the loose transition state assumed here. Oddly, the entropy of activation for dissociation of $K^+(NH_3)_5$ is negative. Upon further inspection, this appears to be a consequence of the very low frequencies of this complex: five torsional modes and two frequencies at 9 cm^{-1} (Table 1), which are associated with hindered translations of the equatorial ligands: one being an in-plane wag of one of the three ammonias, the other being an in-plane scissors motion of the other two ammonias.

3.2. Theoretical geometries

The configurations for the five potassium cation clusters studied by CID were calculated as described above. All ionic clusters favor the most symmetric conformation of the ligands about the central potassium. As expected, the lone pairs of electrons on the ammonia ligands prefer to point towards the potassium ion such that the dipole moment is directed at the cation. Details of the calculated geometries are given in Table 4 and also displayed in Fig. 4. In the following, relative energies are all calculated at the MP2(full)6-311+G(2d,2p)//MP2(full)6-31G(d) level of theory and include zero point energies and BSSE corrections.

For the single ligand complex, the geometry has C_{3v} symmetry, as might be anticipated. Addition of a second ammonia occurs 180° away from the first ligand, such that the two ligands can have an eclipsed geometry (D_{3h}) or a staggered conformation (D_{3d}). Our calculations find that these geometries are separated by less than 0.005 kJ/mol with the staggered D_{3d} structure being lower in energy. This energy barrier demonstrates that the torsional vibration associated

Table 4
MP2(full)/6-31G(d) geometry optimized structures of $K^+(NH_3)_x$ ($x = 1$–5) complexes[a]

Reactant ion	Symmetry	K^+–N distances (Å)	∠N–K^+–N (°)	∠K^+–N–H (°)
$K^+(NH_3)$	C_{3v}	2.793 (1)		113.8 (3)
$K^+(NH_3)_2$	D_{3h}	2.834 (2)	180.0 (1)	113.6 (6)
$K^+(NH_3)_3$	C_{3h}	2.862 (3)	120.0 (3)	113.4 (3)
				113.5 (6)
$K^+(NH_3)_4$	T_d	2.895 (4)	109.5 (6)	113.3 (12)
$K^+(NH_3)_5$	C_{3h}	2.933 (3)	90.0 (6)	113.0 (3)
		2.950 (2)	120.0 (3)	113.3 (6)
			180.0 (1)	113.1 (6)
$K^+(NH_3)_4(NH_3)$	C_s	2.858 (2)	40.4 (2)	113.3 (6)
		2.898 (2)	81.0 (1)	117.3 (6)
		4.958 (1)	109.0 (1)	112.5 (2)
			116.3 (4)	114.5 (1)
			125.5 (2)	

[a] Numbers in parentheses refer to the number of atoms at this distance or angle.

with rotation of the ammonia ligands in opposite directions about the N–K–N axis is accurately treated as a free rotation.

The ground state geometry of the $K^+(NH_3)_3$ complex has all three nitrogen atoms in a plane about the potassium with one hydrogen from each ammonia also in this plane, such that the symmetry is C_{3h}. We investigated how the energy changes upon small perturbations in the symmetry of the complex, specifically with regard to rotations of the ammonia ligands. We find that the barrier to rotation is small (<0.1 kJ/mol), again indicating that the three torsional motions of the ammonia ligands rotating about the K–N axes are best viewed as free rotors.

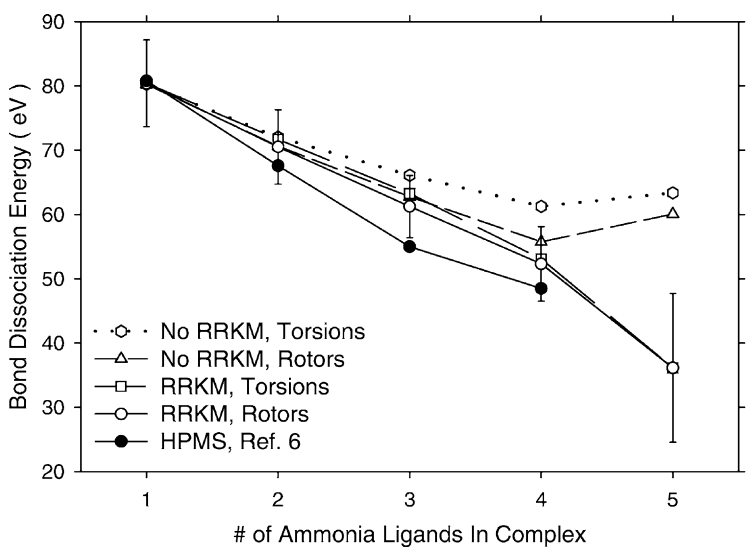

Fig. 4. Bond dissociation energies at 0 K for $K^+(NH_3)_x$ where $x = 1$–5 obtained using four different models (all with the average rate constant model) with Eq. (1): lifetime effects are either excluded (no RRKM) or included (RRKM); torsional motions are treated as vibrations (torsions) or rotors. All these data are taken from Table 3. High-pressure mass spectrometry results from Castleman [6], are shown as closed circles. Experimental error bars (two standard deviations) are included on the (RRKM, rotors) experimental results of the present study (open circles).

A similar case is encountered for the complex containing four ammonia molecules, where all four ammonias bind to K^+ through the nitrogen atom in a tetrahedral arrangement. When the hydrogens are considered, there are two structures with high symmetry, C_{2v} and T_d, which are related by a 60° rotation of any two ammonia ligands. The tetrahedral geometry is found to be lower in energy and has no imaginary frequencies, whereas the C_{2v} geometry is higher in energy by only 0.1 kJ/mol and has two imaginary frequencies. This relationship again indicates the free rotor nature of the ligand torsions.

For the complex containing five ammonia molecules, two structures were investigated. The first was a pentagonal bipyramid having three ammonia ligands arranged symmetrically in a plane, as for the $K^+(NH_3)_3$ complex, with two additional axial ammonias aligned perpendicular to these. The optimal orientation of the hydrogens on the axial ligands maintains C_{3h} symmetry with the hydrogens directed between the equatorial ligands. This geometry had no imaginary frequencies although there were five low frequency torsional motions plus the hindered translations noted above. In part because there was a sharp decrease in intensity of the $K^+(NH_3)_5$ ions compared to the smaller complexes, we also considered a structure in which four ammonias complete the first solvation shell with the fifth ligand hydrogen-bonded in a second shell. A converged structure for such a complex having no imaginary frequencies was found. Here the fifth ligand is hydrogen bonded to two of the four ligands in the first solvation shell, such that the complex has C_s symmetry (Fig. 4). The C_s hydrogen bonded structure is calculated to lie 10 kJ/mol higher in energy than the C_{3h} configuration. At 298 K, the relative free energies give a similar difference of 16 kJ/mol.

As can be seen in Table 4, the metal–ligand bond distances gradually increase as the number of ligands increases. This is consistent with the overall weakening of the metal-ligand bonds with an increase in

Table 5
Bond dissociation energies at 0 K of $K^+(NH_3)_x$ ($x = 1$–5) complexes (in kJ/mol)

Bond	This work						Literature	
	CID[a]	MP2//MP2[b]	B3LYP//B3LYP[b]	MP2//B3LYP[b]	HW[c]	S.D.[d]	HPMS[e]	Theory
K^+–(NH_3)	79 ± 7	72 (*75*)	74 (*74*)	73 (*75*)	61 (*64*)	63 (*65*)	81 ± 9	75[f]
							75 ± 8[g]	70[h]
							71 ± 33[i]	70[j]
$(NH_3)_1K^+$–(NH_3)	69 ± 6	62 (*65*)	62 (*63*)	62 (*65*)	56 (*59*)	57 (*60*)	68 ± 9	66[f]
$(NH_3)_2K^+$–(NH_3)	59 ± 5	54 (*57*)	54 (*54*)	54 (*57*)	48 (*51*)	49 (*51*)	56 ± 8	
$(NH_3)_3K^+$–(NH_3)	46 ± 6	45 (*48*)	43 (*44*)	46 (*49*)	41 (*44*)	42 (*44*)	49 ± 8	
$(NH_3)_4K^+$–(NH_3)	31 ± 11	34 (*38*)	29 (*30*)	34 (*38*)	31 (*35*)	32 (*35*)		
$(NH_3)_4K^+$–(NH_3)[k]		24 (*28*)	20 (*21*)	24 (*28*)	22 (*27*)	23 (*27*)		
MAD[l]		5 ± 2, *4 ± 2*	5 ± 2, *4 ± 2*	4 ± 2, *4 ± 2*	10 ± 6, *8 ± 5*	9 ± 5, *8 ± 4*	2 ± 1	

[a] Experimental values from this work. Threshold uncertainties reported as 2σ.
[b] Ab initio calculations using the level shown with basis sets of 6-311+G(2d,2p) for single point calculations and 6-31G(d) for geometry optimizations and frequency determinations. Italics show energies without including corrections for BSSE.
[c] MP2//MP2 calculations using the same basis set as footnote b except for the potassium ion where the Hay–Wadt ECP is used.
[d] MP2//MP2 calculations using the same basis set as footnote b except for the potassium ion where the Stuttgart–Dresden ECP is used.
[e] HPMS values from [6] converted to 0 K values, see Table 6.
[f] Kaupp and Schleyer [13]. Values have been corrected for zero-point energy.
[g] Davidson and Kebarle [5].
[h] Magnusson and Moriarty [14]. Value has been corrected for zero-point energy.
[i] Marinelli and Squires [7].
[j] Berthod and Pullman [12]. Value has been corrected for zero-point energy.
[k] Values for the $K^+(NH_3)_4(NH_3)$ geometry.
[l] Mean absolute deviations from CID experimental values. Values for the $K^+(NH_3)_4(NH_3)$ are excluded. Italics represent MADs for theoretical values without corrections for BSSE.

complex size. Bond angles for K–N–H remain nearly identical for all complexes. The only exceptions to these trends involve the hydrogen bonding C_s complex of $K^+(NH_3)_5$. Here, two of the ligands attached directly to the metal have bond lengths similar to the $x = 3$ complex, whereas the two ligands attached to the metal but engaged in hydrogen bonding to the fifth ligand have bond lengths like the $x = 4$ complex. Here, the perturbation of the hydrogen bonding is evident in the K–N–H bond angles.

3.3. Theoretical bond energies

Bond energies calculated as described above including ZPE and BSSE corrections are listed in Table 5. Values without BSSE are also listed. Overall, the trends in all these values are similar, although the values involving ECPs are systematically smaller than the other values. Theoretical literature references pertaining to the potassium ammonia systems use a range of different methods to calculate binding energies. For $K^+(NH_3)$, Berthod and Pullman [12] performed SCF calculations keeping the ligand geometry fixed and employing the basis set described by Wachters [58] for potassium. Kaupp and Schleyer [13] did Hartree Fock calculations on both $K^+(NH_3)$ and $K^+(NH_3)_2$ using a quasi-relativistic energy-adjusted pseudopotential for potassium. The most recent investigation of $K^+(NH_3)$ was by Magnusson and Moriarty [14], who gave energies at the MP2 level and used a 6-311+G(d,p) basis for N and H and a metal basis again derived from Wachters [58] by Rosi and Bauschlicher [59,60]. None of these studies included ZPE or BSSE corrections. To facilitate comparison with the values calculated here, Table 5 reports the literature values corrected for these zero point energies: 7 kJ/mol in the case of $K^+(NH_3)$ and 6 kJ/mol for $K^+(NH_3)_2$.

4. Discussion

4.1. Comparison of theoretical and experimental bond energies

As seen in Fig. 5, the bond dissociation energies obtained through CID or HPMS and our theoretical results qualitatively follow similar trends. The bond

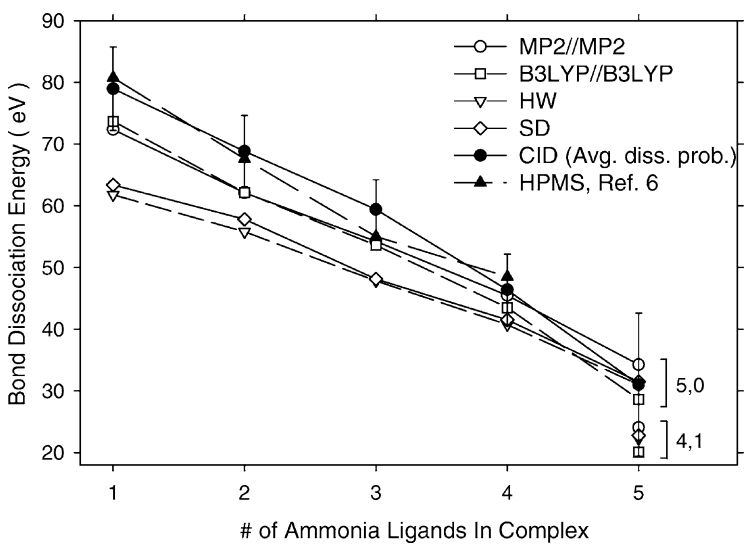

Fig. 5. Comparison of experimental (closed symbols) bond dissociation energies at 0 K for $K^+(NH_3)_x$ where $x = 1$–5 from both the present CID data (RRKM, rotors, average dissociation probability) and HPMS results of Castleman [6], with theoretical results (open symbols) at several levels of theory taken from Table 5.

energies decrease monotonically and are seen to do so at approximately the same rate for all theoretical methods. In general, the theoretical trends reproduce the CID data better than the HPMS data, but absolute theory values for $x = 3$ and 4 better reproduce the HPMS results.

The three theoretical methods used here with all-electron basis sets, MP2//MP2, B3LYP//B3LYP, and MP2//B3LYP, provide very similar results. For example, the two methods employing MP2 single point energies both show good agreement with both the HPMS results, $MAD_{HPMS} = 4 \pm 3$ kJ/mol, and with our CID results, $MAD_{CID} = 4 \pm 2$ kJ/mol. The B3LYP//B3LYP values show similar agreement, $MAD_{HPMS} = 5 \pm 2$ kJ/mol and $MAD_{CID} = 5 \pm 2$ kJ/mol. Thus, there is little to distinguish these three methods. However, if the BSSE corrections are eliminated, B3LYP energies change very little (about 1 kJ/mol), whereas the MP2 energies change by about 3 kJ/mol. These changes lead to slightly better agreement with the experimental results, $MAD_{HPMS} = 3 \pm 2$ kJ/mol and $MAD_{CID} = 4 \pm 2$ kJ/mol.

The ECP calculations show very similar agreement with each other: Hay–Wadt, $MAD_{HPMS} = 12 \pm 5$ kJ/mol and $MAD_{CID} = 10 \pm 6$ kJ/mol, whereas Stuttgart–Dresden, $MAD_{HPMS} = 10 \pm 4$ kJ/mol and $MAD_{CID} = 9 \pm 5$ kJ/mol. Ignoring BSSE corrections improves the agreement slightly (to MAD_{CID} of about 8 kJ/mol), but the ECP calculations are systematically low and do not reproduce the experimental trends as well as the all-electron calculations.

For the $K^+(NH_3)_5$ complex, the theoretical calculations clearly indicate that the experimental results are most consistent with the complex in which all five ligands are attached directly to the potassium ion. The 4,1 complex, in which one of the ligands is in the second solvent shell, is calculated to be less stable by 10 kJ/mol, less consistent with the experimental results than the 5,0 complex. Experimentally, it is possible that ions having both structures are formed in our flow tube source. However, our threshold measurements should be sensitive to the most weakly bound of these if they are both present in reasonable amounts. Therefore, the good agreement between theory for the 5,0 complex and our experimental threshold suggests that the 5,0 structure is formed predominantly.

The few theoretical values available for these systems in the literature [12–14] are also given in Table 5. Reasonable agreement is observed in all cases, with the values of Kaupp and Schleyer [13] being very close to the present theoretical values.

In addition to the HPMS results from Castleman, there are two additional experimental values available in the literature for $K^+(NH_3)$ (Table 5). The earlier HPMS study of Davidson and Kebarle [5] provides a slightly lower value for the bond energy of this complex, but one within the experimental uncertainties. The early CID work of Marinelli and Squires [7] agrees with the other determinations within its larger uncertainty.

4.2. Conversion from 0 to 298 K

In order to facilitate comparison of our CID 0 K values for the bond dissociation energies (BDEs) with other commonly used experimental conditions, conversions are done to convert to 298 K bond enthalpies and free energies (Table 6). These conversions use the frequencies calculated at the MP2(full)/6-31G(d) level under the rigid rotor/harmonic oscillator approximation. Uncertainties in these values are determined by scaling the vibrations ±10% for non-metal ligand frequencies and by a factor of one-half and two for metal ligand frequencies, usually the lowest energy frequencies. The torsional modes are treated as rotors, with the associated rotational constants scaled by factors of one-half and two.

For the $K^+(NH_3)_x$, $x = 1$–4 complexes, the calculated entropy corrections can be compared directly with values obtained by Davidson and Kebarle [5] and Castleman [6], also listed in Table 6. It can be seen that the calculated entropies of dissociation agree with the experimental values quite nicely. In this regard, it is useful to note that if these entropies are calculated using alternate molecular parameters (those in which the torsions are treated as vibrations), the $T\Delta S_{298}$ values for $x = 2$–4 are about 6 ± 1 kJ/mol lower than

Table 6
Enthalpies and free energies for $(NH_3)_{x-1}K^+$–NH_3 at 0 and 298 K in kJ/mol[a]

System	ΔH_0		$\Delta H_{298} - \Delta H_0^c$	ΔH_{298}		$T\Delta S_{298}$		ΔG_{298}	
$K^+(NH_3)$	79 ± 7[b]	**81 ± 9**, *71 ± 9*	3.3 ± 3.7	82 ± 8	**84 ± 8**, *75 ± 8*	27 ± 8[c]	**29 ± 5**, *25 ± 5*	55 ± 11	**55 ± 9**, *49 ± 8*
$K^+(NH_3)_2$	69 ± 6[b]	**68 ± 9**	0.6 ± 3.9	70 ± 7	**68 ± 8**	27 ± 17[c]	**28 ± 5**	42 ± 18	**40 ± 9**
$K^+(NH_3)_3$	59 ± 5[b]	**55 ± 9**	1.5 ± 3.8	61 ± 6	**56 ± 8**	29 ± 15[c]	**29 ± 5**	32 ± 17	**27 ± 9**
$K^+(NH_3)_4$	46 ± 6[b]	**49 ± 9**	0.0 ± 4.2	46 ± 7	**49 ± 8**	36 ± 16[c]	**32 ± 5**	11 ± 18	**17 ± 9**
$K^+(NH_3)_5$	31 ± 11[b]		−1.0 ± 1.8	30 ± 12		22 ± 19[c]		8 ± 22	
$K^+(NH_3)_4(NH_3)$	22[d]		1.6 ± 6.5	24 ± 7		31 ± 19[c]		−7 ± 20	

[a] In all cases, uncertainties are listed as 2σ, roman values are from this work, HPMS values from Castleman [6] are in bold, and those in italics are from Davidson and Kebarle [5]. Uncertainties (2σ) for the HPMS values have been estimated as 8 kJ/mol (2σ) as per [5].
[b] Experimental values from this work (Table 5).
[c] Values were computed using standard formulas and molecular constants calculated at the MP2(full)/6-31G(d) level. The uncertainties correspond to 10% variations in the vibrational frequencies of the ligands and two-fold variations in the metal ligand-frequencies and rotational constants for the torsional modes.
[d] Average theoretical value from Table 5.

the values listed in Table 6. (The value for $x = 1$ is the same because there are no torsions.) Thus, when the torsions are treated as vibrations, the agreement with the experimental values is worse, although still within the estimated uncertainties. This comparison to experimentally determined entropies provides another reason to believe that the treatment of the torsional motions as rotors is more appropriate than as vibrations.

Finally, we note that the entropic corrections calculated for the two structures of $K^+(NH_3)_5$ are quite distinct and lead to a free energy difference between the two structures of 15 kJ/mol (Table 6). It seems clear that an equilibrium study on this complex would be able to confirm the theoretical prediction regarding the ground state geometry.

5. Conclusion

Bond dissociation energies for the $K^+(NH_3)_x$ (x = 1–5) are determined using threshold CID. These experimental values are displayed in Table 6 and Fig. 5. The results are in excellent agreement with HPMS results of Davidson and Kebarle [5] for $K^+(NH_3)$ and Castleman [6] for $K^+(NH_3)_x$ (x = 1–4). The results agree reasonably with ab initio theoretical calculations at the several levels of theory but values calculated using ECPs are systematically low. These calculations indicate that the geometries of the ligands prefer the most symmetrical configuration available in all five complexes.

Evaluation of the treatments of torsions as vibrations or rotors suggests that better agreement with both literature and theory is obtained by including these modes as rotors in our analysis of the CID data. This was true in comparisons of absolute bond energies and entropies of dissociation, although differences are within experimental uncertainties. Addition of the ion–dipole potential to the treatment of the transition state had little effect on the threshold modeling for these complexes although it systematically reduces the kinetic shift. Further investigation of the dipole effects would be useful especially with complexes that have a larger dipole moment than ammonia. We also considered whether anharmonicities of the vibrations corresponding to the "frustrated translations" leading to dissociation might influence the thresholds measured but found negligible differences for all cluster sizes. Finally, we examined two models for the 2D external rotations of the energized complexes, average rate constant and average dissociation probability. The latter model leads to slightly larger kinetic shifts than the former model, thereby providing slightly

better agreement of the CID thresholds with the HPMS bond energies.

Acknowledgements

This work was supported by the National Science Foundation, Grant No. CHE-013557. C.I. thanks J.C. Amicangelo for helpful discussions. PBA thanks Prof. Kent Ervin for useful discussions and continued collaboration on enhancing the Crunch analysis program used throughout the present data analysis.

References

[1] J. Brickmann, A. Skerra, in: H. Kleeberg (Ed.), Interactions of Water Ionic Nonionic Hydrates, Springer, Berlin, Fed. Rep. Ger., Darmstadt, Fed. Rep. Ger., 1987, p. 217.
[2] K.A. Duca, P.C. Jordan, Biophys. Chem. 65 (1997) 123.
[3] M. Poxleitner, J. Seitz-Beywl, K. Heinzinger, in: Proceedings of the Italian Physics Society Conference, 1993.
[4] S.B. Rempe, L.R. Pratt, Book of Abstracts, 219th ACS National Meeting, American Chemical Society, Washington, DC, 2000.
[5] W.R. Davidson, P. Kebarle, J. Am. Chem. Soc. 98 (1976) 6133.
[6] A.W. Castleman Jr., Chem. Phys. Lett. 53 (1978) 560.
[7] P.J. Marinelli, R.R. Squires, J. Am. Chem. Soc. 111 (1989) 4101.
[8] S. Suzer, L. Andrews, J. Am. Chem. Soc. 109 (1987) 300.
[9] J.C. Amicangelo, P.B. Armentrout, J. Phys. Chem. A 104 (2000) 11420.
[10] M.T. Rodgers, P.B. Armentrout, J. Phys. Chem. A 104 (2000) 2238.
[11] M.T. Rodgers, P.B. Armentrout, J. Phys. Chem. A 101 (1997) 2614.
[12] H. Berthod, A. Pullman, Chem. Phys. Lett. 70 (1980) 434.
[13] M. Kaupp, P.V. Schleyer, J. Phys. Chem. 96 (1992) 7316.
[14] E. Magnusson, N.W. Moriarty, J. Phys. Chem. 98 (1994) 12558.
[15] K.M. Ervin, P.B. Armentrout, J. Chem. Phys. 83 (1985) 166.
[16] R.H. Schultz, P.B. Armentrout, Int. J. Mass Spectrom. Ion Process. 107 (1991) 29.
[17] F. Muntean, P.B. Armentrout, J. Chem. Phys. 115 (2001) 1213.
[18] R.H. Schultz, K.C. Crellin, P.B. Armentrout, J. Am. Chem. Soc. 113 (1992) 8590.
[19] R.H. Schultz, P.B. Armentrout, J. Chem. Phys. 96 (1992) 1046.
[20] F.A. Khan, D.E. Clemmer, R.H. Schultz, P.B. Armentrout, J. Phys. Chem. 97 (1993) 7978.
[21] E.R. Fisher, B.L. Kickel, P.B. Armentrout, J. Phys. Chem. 97 (1993) 10204.
[22] N.F. Dalleska, K. Honma, P.B. Armentrout, J. Am. Chem. Soc. 115 (1993) 12125.
[23] E. Teloy, D. Gerlich, Chem. Phys. 4 (1974) 417.
[24] T.S. Beyer, D.F. Swinehart, Comm. Assoc. Comput. Machines 16 (1973) 379.
[25] S.E. Stein, B.S. Rabinovitch, J. Chem. Phys. 58 (1973) 2438.
[26] S.E. Stein, B.S. Rabinovitch, Chem. Phys. Lett. 49 (1977) 1883.
[27] R.G. Gilbert, S.C. Smith, Theory of Unimolecular and Recombination Reactions, Blackwell, Oxford, UK, 1990.
[28] J.A. Pople, H.B. Schlegel, K. Raghavachari, D.J. DeFrees, J.F. Binkley, M.J. Frisch, R.F. Witesides, R.F. Hout, W.J. Hehre, Int. J. Quantum Chem. Symp. 15 (1981) 269.
[29] D.J. DeFrees, A.D. McLean, J. Chem. Phys. 82 (1985) 333.
[30] M.T. Rodgers, K.M. Ervin, P.B. Armentrout, J. Chem. Phys. 106 (1997) 4499.
[31] E.V. Waage, B.S. Rabinovitch, Chem. Rev. 70 (1970) 377.
[32] V.F. DeTuri, K.M. Ervin, JPCA 103 (1999) 6911.
[33] W.J. Chesnavich, M.T. Bowers, J. Phys. Chem. 68 (1978) 901.
[34] P.B. Armentrout, in: N. Adams, L.M. Babcock (Eds.), Advances in Gas Phase Ion Chemistry, vol. 1, JAI Press, Greenwich, 1992, p. 83.
[35] L.S. Sunderlin, P.B. Armentrout, Int. J. Mass Spectrom. Ion Process. 94 (1989) 149.
[36] M.T. Rodgers, P.B. Armentrout, J. Phys. Chem. 101 (1997) 1238.
[37] N.F. Dalleska, K. Honma, L.S. Sunderlin, P.B. Armentrout, J. Am. Chem. Soc. 116 (1994) 3519.
[38] M.B. More, E.D. Glendening, D. Ray, D. Feller, P.B. Armentrout, J. Phys. Chem. 100 (1996) 1605.
[39] M.B. More, D. Ray, P.B. Armentrout, J. Phys. Chem. 101 (1997) 831.
[40] D. Ray, D. Feller, M.B. More, E.D. Glendening, P.B. Armentrout, J. Phys. Chem. 100 (1996) 12866.
[41] P.B. Armentrout, J. Simons, J. Am. Chem. Soc. 114 (1992) 8627.
[42] M.J. Frisch, G.W. Trucks, H.B. Schlegel, G.E. Scuseria, M.A. Robb, J.R. Cheeseman, V.G. Zakrzewski, J.A. Montgomery Jr., R.E. Stratmann, J.C. Burant, S. Dapprich, J.M. Millam, A.D. Daniels, K.N. Kundin, M.C. Strain, O. Farkas, J. Tomasi, V. Barone, M. Cossi, R. Cammi, B. Mennucci, C. Pomelli, C. Adamo, S. Clifford, J. Ochterski, G.A. Petersson, P.Y. Ayala, Q. Cui, K. Morokuma, D.K. Malick, A.D. Rabuck, K. Raghavachari, J.B. Foresman, J. Cioslowski, J.V. Ortiz, B.B. Stefanov, G. Liu, A. Liashenko, P. Piskorz, I. Komaromi, R. Gomperts, R.L. Martin, D.J. Fox, T. Keith, M.A. Al-Laham, C.Y. Peng, A. Nanayakkara, C. Gonzalez, M. Challacombe, P.M.W. Gill, B. Johnson, W. Chen, M.W. Wong, J.L. Andres, C. Gonzalez, M. Head-Gordon, E.S. Replogle, J.A. Pople, in: Pople (Ed.), Revision A.7 ed., Gaussian, Inc., Pittsburgh, PA, 1998.
[43] C. Møller, M.S. Plesset, Phys. Rev. 46 (1934) 618.
[44] R.J. Bartlett, Annu. Rev. Phys. Chem. 32 (1981) 359.

[45] W.J. Hehre, L. Radom, P.v.R. Schleyer, J.A. Pople, Ab initio Molecular Orbital Theory, Wiley, New York, 1986.
[46] S. Hoyau, K. Norrman, T.B. McMahon, G. Ohanessian, J. Am. Chem. Soc. 121 (1999) 8864.
[47] A. Andersen, F. Muntean, D. Walter, C. Rue, P.B. Armentrout, J. Phys. Chem. A 104 (2000) 692.
[48] J.B. Foresman, A. Frisch, Exploring Chemistry with Electronic Structure Methods, 2nd ed., Gaussian Inc., Pittsburg, PA, 1996.
[49] S.F. Boys, R. Bernardi, Mol. Phys. 19 (1970) 553.
[50] F.B. van Duijneveldt, J.G.C.M. van Duijneveldt, J.H. van Lenthe, Chem. Rev. 94 (1994) 1873.
[51] P.J. Hay, W.R. Wadt, J. Chem. Phys. 82 (1985) 299.
[52] D. Andrae, U. Haeussermann, M. Dolg, H. Stoll, H. Preuss, Theor. Chim. Acta 77 (1990) 123.
[53] A.D. Becke, J. Chem. Phys. 98 (1993) 5648.
[54] C. Lee, W. Yang, R.G. Parr, Phys. Rev. B 37 (1988) 785.
[55] N. Aristov, P.B. Armentrout, J. Phys. Chem. 90 (1986) 5135.
[56] D.A. Hales, P.B. Armentrout, J. Cluster Sci. 1 (1990) 127.
[57] E.W. Rothe, R.B. Bernstein, J. Chem. Phys. 31 (1959) 1619.
[58] A.J.H. Wachters, J. Chem. Phys. 52 (1970) 1033.
[59] M. Rosi, C.W. Bauschlicher Jr., J. Chem. Phys. 90 (1989) 7264.
[60] M. Rosi, C.W. Bauschlicher Jr., J. Chem. Phys. 92 (1990) 1876.